

# Global observation-based reconstruction of previous-century irrigation-induced cooling

Wageningen University MSc Internship Report

Internship provider:

Institute for Atmospheric and Climate Science, ETH Zurich, Zurich, Switzerland

Auke Visser

August 8, 2019

# Contents

<b>1</b>	<b>Introduction</b>	<b>3</b>
<b>2</b>	<b>Research Questions</b>	<b>4</b>
<b>3</b>	<b>Temperature and irrigation data</b>	<b>4</b>
3.1	Observational data . . . . .	4
3.2	Model output . . . . .	5
<b>4</b>	<b>Methods: window searching algorithms</b>	<b>5</b>
4.1	The threshold-based method . . . . .	5
4.2	The regression-based method . . . . .	6
<b>5</b>	<b>Issues related to data sets</b>	<b>7</b>
<b>6</b>	<b>Results</b>	<b>7</b>
6.1	Exploratory analysis . . . . .	7
6.2	Algorithm configuration . . . . .	8
6.2.1	Cooling trend as captured by the algorithm . . . . .	8
6.2.2	Search window size . . . . .	10
6.2.3	Reference period selection . . . . .	11
6.3	Reconstructing the irrigation-induced temperature effect . . . . .	11
6.3.1	CRU . . . . .	11
6.3.2	HadEX2 . . . . .	14
6.4	Comparing CESM model output to CRU observations . . . . .	15
<b>7</b>	<b>Discussion</b>	<b>17</b>
<b>8</b>	<b>Conclusions and Outlook</b>	<b>18</b>
<b>A</b>	<b>Appendices</b>	<b>23</b>
A	Auxiliary figures . . . . .	23
B	Python scripts . . . . .	25
B.1	The window searching algorithms . . . . .	25
B.2	Relevant plotting scripts . . . . .	26

# 1 Introduction

Food production increasingly relies on irrigation, as the 2% of irrigated global land is responsible for 40% of global food production (Bonfils & Lobell, 2007), and irrigable areas have more than tripled in the past century (Siebert *et al.*, 2015). Global climate studies generally do not account for irrigation, as its effects are assumed to be small at the global scale. Understanding irrigation impacts on climate and vice versa is however essential for understanding future regional climate in irrigated areas, and global food security. Additionally, profound impacts on the hydrological cycle such as groundwater depletion (Rodell *et al.*, 2009) raise questions about long-term sustainability of irrigation practices.

Climatic effects of irrigation include a direct cooling effect through enhancement of the surface latent heat flux, and indirect effects related to enhanced atmospheric moisture such as enhanced cloud formation, precipitation or even altered circulation patterns (Puma & Cook, 2010). Because of its limited spatial extent at a global scale, climatic impacts of irrigation have been underrepresented in climate research.

Recent years however saw increased research attention to the quantification of irrigation-induced climate effects. The effect of irrigation on surface temperature has been assessed by various observational (Bonfils & Lobell, 2007; Lobell *et al.*, 2008; Mahmood *et al.*, 2013; Shi *et al.*, 2014; Mueller *et al.*, 2015) and modeling (Kueppers *et al.*, 2007; Sacks *et al.*, 2009; Puma & Cook, 2010; Shukla *et al.*, 2014; Thiery *et al.*, 2017) efforts. The most important observational conclusion thus far is that irrigated areas experience dampened trends in hot temperature extremes compared to their non-irrigated surroundings (see Table 1). The heterogeneity of quantification methods is an important downside to these studies.

The spatial extents of model- and observation-based analyses do not overlap: observational studies often focus on hydrological catchment-scale regions, whereas most model-based studies aim to study irrigation impacts using regional or global climate models. Global modeling studies are important for quantifying the irrigation-induced temperature from a process-based perspective, and can additionally assess future impacts of irrigation (Cook *et al.*, 2011). However, their performance in simulating irrigation-induced climate effects has so far not been tested in a comprehensive way.

The recent transient irrigated area data set spanning the 20<sup>th</sup> century (Siebert *et al.*, 2015) and increased coverage and resolution of global temperature data sets (e.g. Harris *et al.*, 2014) allow for a global assessment of the surface temperature response to irrigation. Additionally, the global assessment can uncover climate effects of irrigation in areas currently underrepresented in observational assessments, such as South Asia. This study thus aims to assess irrigation-induced cooling from gridded observational data sets at the global scale. In particular, a window searching algorithm is applied that was previously used to study climate impacts of deforestation (Kumar *et al.*, 2013; Li *et al.*, 2015; Lejeune *et al.*, 2016, 2017) to compare temperature changes over the past century in irrigated cells versus non-irrigated cells in a rectangular box around the cell of interest. The algorithm is applied to temperature extremes from CRU (Harris *et al.*, 2014) and HadEX2 (Donat *et al.*, 2013) to quantify irrigation-induced cooling in the previous century.

Table 1: Observation-based estimates of irrigation impacts on surface temperature change. The column ' $\Delta T_{irr}$  estimate' contains the median or the range between the lowest and highest estimate.

Source	Region	$\Delta T_{irr}$ estimate	$f_{irr}$ threshold	Method	$T$ index
Mueller <i>et al.</i> (2015)	US Midwest	-0.12 per decade	3-5% per decade	quantile regression	TXx
Lobell <i>et al.</i> (2008)	California, Nebraska	-0.15 per decade	>50% PD	pairwise station comparison	Top 30 TX
Mahmood <i>et al.</i> (2013)	High Plains aquifer	-1.57 - 5.75	County-level maxima	pairwise station comparison	$\overline{T}_{max,GS}$
Shi <i>et al.</i> (2014)	East China	-0.18 per decade	>50% PD	pairwise station comparison	Top 30 TX
Bonfils & Lobell (2007)	California	-0.25 - -0.14 per decade	>50% PD	gridded T products	JJA $\overline{T}_{max}$

## 2 Research Questions

The following research questions have been formulated:

1. The search window approach has been previously applied to climate model output (Kumar *et al.*, 2013; Lejeune *et al.*, 2016, 2017) and to satellite land surface temperature observations (Li *et al.*, 2015), but not to gridded point source observations. Can a search window algorithm be applied to observational temperature estimates to quantify irrigation-induced cooling?
2. Can the algorithm configuration be modified to improve the quantification of the observed direct climate effects of irrigation?
3. By how much has irrigation affected mean and extreme near-surface temperatures in the previous century, and in which regions?
4. How do irrigation estimates simulated by CESM and observed from CRU compare?

## 3 Temperature and irrigation data

### 3.1 Observational data

This analysis relies on temperature and irrigation data to detect differential temperature change signals between irrigated cells and their non-irrigated surroundings in the previous century. Temperature data is taken from CRU TS v3.22 (Harris *et al.*, 2014), which contains estimates of monthly averaged mean temperature, diurnal temperature range, maximum temperature and minimum temperature at a spatial resolution of  $0.5^\circ \times 0.5^\circ$  between 1900 and 2013. The former two products are gridded from station observations. Minimum and maximum temperatures are derived from mean temperature and diurnal temperature range, assuming a symmetric temperature distribution centered around the mean. A temperature extremes metric has been calculated from CRU data as irrigation has been shown to affect hot temperature extremes (e.g. Lobell *et al.*, 2008; Shi *et al.*,

2014; Mueller *et al.*, 2015; Thiery *et al.*, 2017). The temperature product used here is the average maximum temperature in the hottest month of the year ( $TMX_{max}$ ). This metric has been averaged for two 30-year periods in order to calculate the irrigation-induced temperature change effect between the present-day (1981-2010) and the previous century (1901-1930).

For the analyses with HadEX2 (Donat *et al.*, 2013), the analysis uses the annual maximum daytime temperature ( $TX_x$ ). HadEX2 is a gridded dataset of temperature extremes at a resolution of  $3.75^\circ \times 2.5^\circ$ . The data spans the period 1901-2010, although data coverage is limited in heavily irrigated areas in India in the first half of the previous century.

Irrigated area data is derived from the Historical Irrigation Dataset (HID) by Siebert *et al.* (2015), who compiled area equipped for irrigation data based on national and sub-national statistics at a spatial resolution of  $5' \times 5'$  and a temporal resolution of 10 years, increasing to 5 years after 1980. We note that this dataset reflects irrigation infrastructure in place, which might differ from the actually irrigated area. Area equipped for irrigation has been converted to irrigable cell fraction and subsequently remapped to CRU resolution using second-order conservative remapping.

### 3.2 Model output

Simulations of the irrigation-induced temperature effect have been performed with the GCM Community Earth System Model (CESM) with a set-up described in Thiery *et al.* (2017). A subsequent ensemble simulation with no prescribed irrigation for 1901-1930 was performed in order to compare the simulated irrigation-induced temperature effect with observations over the 20<sup>th</sup> century. The present-day irrigation on climate has been simulated using a global irrigation map for the year 2000 (Siebert *et al.*, 2005).

## 4 Methods: window searching algorithms

The two window searching strategies applied here identify contrasting temperature trends in irrigated cells and their non-irrigated direct surroundings. They are designed to differentiate between homogeneous climate forcings such as enhanced greenhouse gas concentrations and heterogeneously distributed local climate drivers such as irrigation. The algorithms have been adapted from previous studies focused on deforestation (Kumar *et al.*, 2013; Lejeune *et al.*, 2017; Li *et al.*, 2015; Lejeune *et al.*, 2016).

### 4.1 The threshold-based method

This method, adapted from Kumar *et al.* (2013) and Lejeune *et al.* (2016) consists of three steps:

1. Pixel selection: Irrigated pixels are selected for analysis if they exceed an irrigated fraction threshold value in the present-day. Additionally, we require that at least 30% of the cells in a  $15 \times 15$  box surrounding these cells are land-based. In order to limit the effect of outliers in the temperature dataset on the reconstructed irrigation-induced temperature impact, at least 10% of these cells exceed the present-day irrigation threshold, and at least 10% of the cells do not exceed the present-day threshold. When the data availability conditions are not satisfied, these conditions are successively tested in bigger boxes of  $17 \times 17$  cells and  $17 \times 19$  cells.

The pixel selection differs slightly from Lejeune *et al.* (2016), where pixels were selected based on land cover changes rather than present-day land cover. Looking at present-day irrigated fraction changes however enables us to study the effect of large irrigated fractions, where the largest irrigation-impact on temperature is expected. Additionally, changes in irrigated area

reached a historic maximum in the previous century ([Siebert et al. , 2015](#)), which means that areas with high present-day irrigated fractions are expected to show large changes in irrigated areas in the previous century.

2. Pixel separation: An irrigation effect on surface temperature trends is hypothesized to occur when the irrigation extent in a grid cell of interest has increased over the past century. Therefore, cells inside the search window are divided into irrigated and non-irrigated cells based on the irrigation evolution in the previous century. At least 50% of the present-day irrigated area must have been added in the previous century. Cells that do not meet this criterion are considered non-irrigated.
3. Irrigation impact reconstruction: The temperature effect of irrigation in the irrigated cell of interest is calculated as the difference between the mean temperature changes in irrigated versus non-irrigated cells:

$$\overline{\Delta T_{irr}} = \overline{\Delta T}_{\Delta f_{irr} \geq v} - \overline{\Delta T}_{\Delta f_{irr} < v} \quad (1)$$

where  $v$  is calculated from the present-day irrigation threshold for pixel selection  $t_{irr,PD}$  as

$$v = 0.5 \times t_{irr,PD} \quad (2)$$

## 4.2 The regression-based method

The reconstructed temperature effect from the threshold-based method is potentially impacted by the choice for the irrigated fraction threshold. [Lejeune et al. \(2017\)](#) therefore developed a multi-linear regression-based method which is not dependent on this threshold.

1. Pixel selection: Pixels exceeding a present-day irrigation threshold are selected for analysis if a window of  $15 \times 15$  cells centered around the pixel of interest has a data coverage of at least 60%, and if at least 8% of the pixels are irrigated. The selection criteria match those by [Lejeune et al. \(2017\)](#), with the exception of the search window size which is larger in the present study. A larger search window increased the temperature contrast between irrigated cells and their surroundings (which is hypothesized to be due to the clustered spatial irrigation pattern, see Section 6.2.2 for more details), but smoothes the signal compared to smaller windows.
2. Multi-linear regression: the analysis extracts an irrigation-induced temperature signal by performing a multi-linear regression on all pixels in the search windows. The regressors are the change in irrigated fraction and, analogous to [Lejeune et al. \(2017\)](#), three spatial predictors which may confound the irrigation-derived signal (latitude, longitude and elevation). This results in the following multi-linear regression model:

$$\Delta T = \alpha_1 \times \Delta f_{irr} + \alpha_2 \times lat. + \alpha_3 \times lon. + \alpha_4 \times elev. \quad (3)$$

3. Irrigation impact reconstruction: the multi-linear regression coefficient for irrigation obtained from Equation 3 is multiplied by the change in irrigated fraction in the cell of interest:

$$\Delta T_{irr} = \alpha_1 \times \Delta f_{irr} \quad (4)$$

The algorithm is designed to capture the direct cooling effect of irrigation due to an enhanced surface latent energy flux. The secondary effects of irrigation such as enhanced atmospheric moisture content potentially leading to downwind precipitation and altered monsoon circulation (Puma & Cook, 2010; Guimberteau *et al.*, 2012; Thiery *et al.*, 2017) are potential confounding factors because they act more or less heterogeneously in the search window. Additionally, this method does not correct for possible dependence between spatial predictors. For example, most irrigation occurs in low-lying areas. This spatial dependence could reduce the regression coefficient for irrigation and thus  $\Delta T_{irr}$  (see Section 7).

## 5 Issues related to data sets

Several features of the used data sets limit their suitability to quantify irrigation-induced temperature effects. Harris *et al.* (2014) obtain a global coverage for CRU by assuming a spatial footprint of climate indices (i.e. a range within which information can be drawn from a point observation) and subsequently interpolating station observations to a regular grid. This potentially results in spatial dependence between neighboring grid cells. A second point of consideration is the arithmetic nature of the maximum monthly temperature product in CRU ( $TMX$ ). This metric, used to calculate the temperature extremes metric  $TMX_{max}$ , is obtained as the sum of the mean temperature and half of the diurnal temperature range. It follows that temperature extremes may not be captured accurately by this index.

Two considerations should be borne in mind regarding the applicability of the HID data set to quantify temperature effects of irrigation. The data set is compiled based on installed irrigation infrastructure rather than actually irrigated land (Siebert *et al.*, 2015). The possibility of unused irrigation infrastructure in certain areas implies that the method may falsely attribute temperature trends to irrigation. An additional consideration is that spatially aggregating HID data to CRU resolution may remove part of the spatial signal in irrigated area.

## 6 Results

### 6.1 Exploratory analysis

Simple visualizations can help to study links between irrigation and surface temperature trends. Before disentangling irrigation-driven changes from the composite temperature effect, it is worthwhile to look at the total temperature change over the past century ( $\Delta T_{tot}$ ). This metric shows the composite effect of global and local climate forcings:

$$\Delta T_{tot} = \Delta T_{anthr} + \Delta T_{irr} + \Delta T_{other} \quad (5)$$

where  $\Delta T_{anthr}$  is the anthropogenic influence on temperature changes,  $\Delta T_{irr}$  is the irrigation impact on temperature changes and  $\Delta T_{other}$  is the temperature change resulting from other forcings (e.g. natural variability, volcanic and solar forcing).

Figure 1 shows decreasing temperature changes with  $f_{irr,PD}$  for the irrigation hot spots South Asia and East Asia. The total temperature change is negative for large changes in irrigated cell area. Other regions show a different picture: a slight decrease in  $\Delta T_{tot}$  can be observed in the Mediterranean, Central North America, West North America and to some extent Southeast Asia, whereas for West Asia no trend can be observed at all. The composite global effect is a decreasing trend, which is affected by East Asia and South Asia particularly for large values of  $f_{irr,PD}$ . This figure implies that the largest signal of irrigation on temperature is expected in East Asia and South

Asia, whereas irrigation effects can less easily be distinguished in the total temperature change signal in other regions.

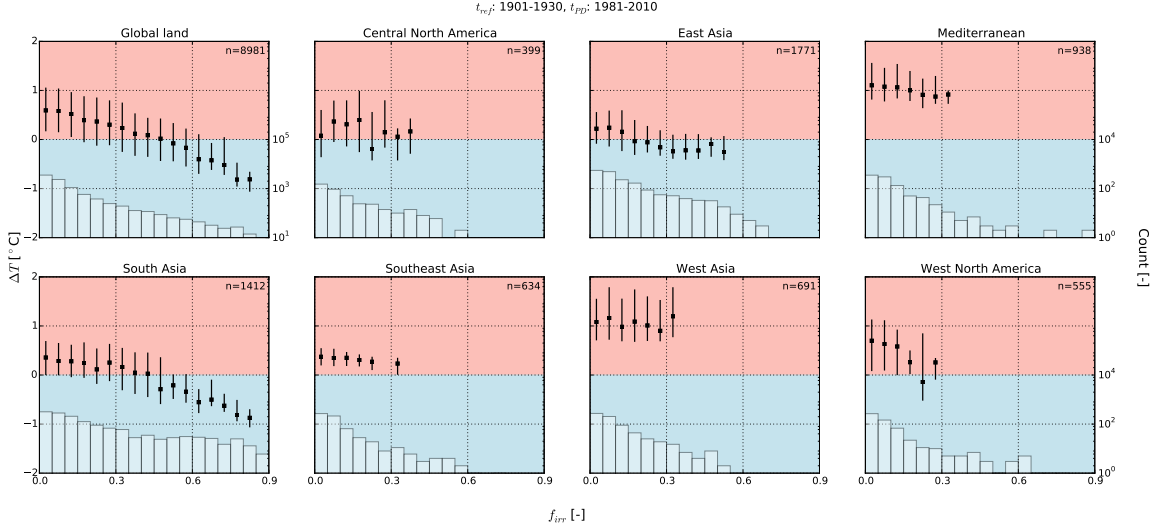


Figure 1: Boxplots of the change in CRU average maximum daytime temperature in the hottest month of the year ( $\Delta T$ ) grouped by changes in irrigated fraction ( $f_{irr,PD}$ ), for global land (top left) and 7 SREX regions containing irrigation. Dots and vertical lines respectively indicate median temperature and the range between the 25<sup>th</sup> and 75<sup>th</sup> percentile for  $\Delta T$  (calculated if  $n_{bin} \geq 10$ ). Cells with a present-day irrigated extent below 2% of the cell area have been omitted for visualization purposes, with a negligible effect on the displayed temperature distributions. Shaded areas indicate warming (red) or cooling (blue) of the cell temperatures grouped by  $f_{irr,PD}$ . The histogram (white vertical bars) contains the cell count.

## 6.2 Algorithm configuration

### 6.2.1 Cooling trend as captured by the algorithm

A series of tests have been performed to determine whether the window search algorithm can correctly capture a cooling signal from temperature observations in irrigated areas. A monotonous trend in the fraction of cooled cells can be observed for both methods (see figure 2), which increases up to 1 for large values of present-day irrigated area. This illustrates the tendency towards cooling for larger irrigated fractions.

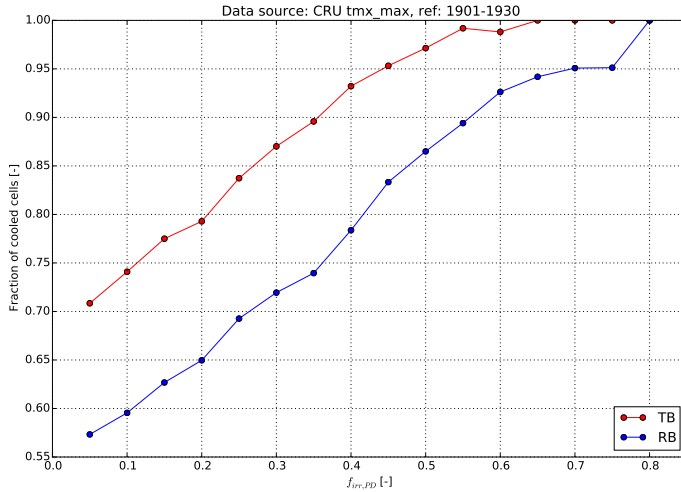


Figure 2: Fraction of cells that show a negative irrigation-induced temperature trend ( $\Delta T_{irr}$ ) in the average maximum daytime temperature in the hottest month of the year between 1901-1930 and 1981-2010.

Figure 3 shows a decreasing  $\Delta T_{irr}$  trend with increasing irrigated fraction. A mean cooling is already found for irrigated fraction thresholds as low as 0.1, but the strength of the cooling effect increases for progressively higher thresholds. Selecting higher thresholds also removes most of the positive outliers, whereas the negative outliers remain. Additionally, the fact that  $\Delta T_{irr}$  cannot be drawn from a normal distribution for any threshold further substantiates that there is a dominant tendency towards cooling of hot temperature extremes for irrigated cells.

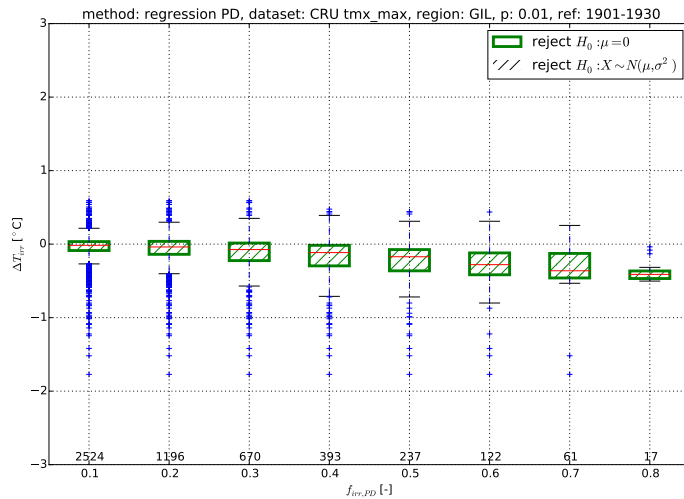


Figure 3: Reconstructed  $\Delta T_{irr}$  for present-day irrigated cell fraction values, using the regression-based method for CRU  $TMX_{max}$  between 1901-1930 and 1981-2010. Colored boxes indicate that  $\Delta T_{irr}$  significantly differs from zero (based on a two-sided one-sample Student's T-test) and hatched boxes indicate a skewed distribution (based on the Shapiro-Wilk normality test), both at a significance level of  $P \leq 0.01$ . The sample size for the reconstructed temperature effect is given at the bottom of the figure.

Previous studies also determined thresholds to distinguish irrigated from non-irrigated cells: model-based studies (e.g. Thiery *et al.*, 2017) used values as low as 10%, whereas most observational studies chose a threshold of 50% (Bonfils & Lobell, 2007; Lobell *et al.*, 2008; Shi *et al.*, 2014). The sensitivity of  $\Delta T_{irr}$  to the irrigation threshold must be determined in order to learn more about the conditions under which climate is influenced by irrigation. The results in Figures 2 and 3 show that irrigation-induced cooling can be detected in observational temperature datasets at low-thresholds, but that the impact on temperature is larger for higher irrigated fraction values. Therefore, as a compromise between the reconstructed temperature effect and sample size, an  $f_{irr,PD}$  value of 0.5 was chosen for the further analysis. This value also improves consistency with previous observation-based studies of irrigation cooling.

### 6.2.2 Search window size

The window searching methods as applied in this study rely on the assumptions that the observed temperature changes resulting from irrigation are strictly local, and that the climate forcing posed by irrigation is spatially heterogeneous (i.e. irrigated pixels are randomly distributed over the search window). The first assumption is violated, because irrigation also has non-local climate impacts. Firstly, locally colder temperatures over irrigated areas might be advected to non-irrigated areas resulting in lower temperature differences than suggested by the irrigation effect. Secondly, enhanced evaporation from irrigated areas adds moisture to the boundary layer, which can cause enhanced cloud formation and precipitation downwind of irrigated areas (Puma & Cook, 2010).

The assumption regarding spatial heterogeneity of the climate forcing is also violated, because irrigation is a clustered phenomenon largely determined by geographical features such as altitude and water supply. This implies that temperature contrasts between irrigated and non-irrigated may not be captured in small search windows, particularly when using high-resolution temperature data.

The impact of both assumption violations can be minimized by increasing the search window size. Increasing the search window size decreases the non-local temperature effects of irrigation and the likelihood that irrigated areas cover most of the search window. The original search window sizes vary between  $5 \times 5$  cells and  $7 \times 9$  cells for search window studies applied to deforestation (Kumar *et al.*, 2013; Lejeune *et al.*, 2016). Increasing the search window to  $11 \times 11$  or  $15 \times 15$  cells increases the contrast between the locally observed cooling (which is independent of the search window size) and the average temperature change in the search window (see Figure 4). It should be noted here that the effective search window size is smaller in this study compared previous studies (e.g. Lejeune *et al.*, 2017, 2016), because those relied on coarser resolution input data.

We note, however, that large search windows lead to over-smoothing of  $\Delta T_{irr}$  because the search windows surrounding adjacent irrigated cells largely overlap. This analysis has only been performed for the CRU temperature product. HadEX2 and CESM search window sizes have been chosen to be in line with those in CRU.

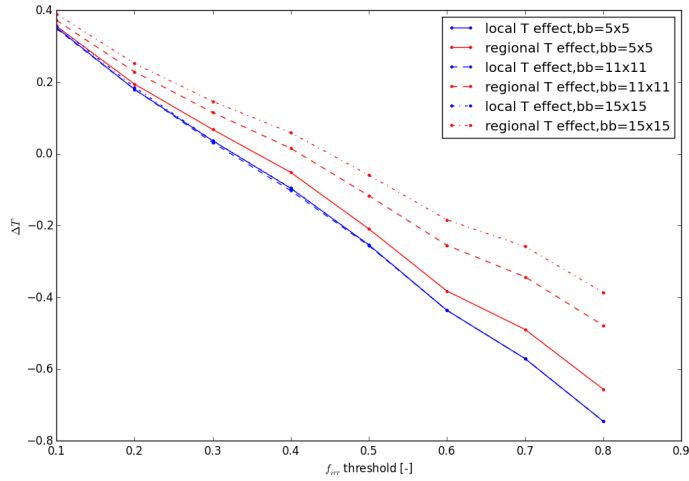


Figure 4: Changes in temperature in local (irrigated cell) and regional (search window) temperature ( $\Delta T_{tot}$ ) as a function of the present-day irrigation threshold for search window sizes of  $5 \times 5$ ,  $11 \times 11$  and  $15 \times 15$  cells.

### 6.2.3 Reference period selection

The window searching method is designed to study differential temperature changes in irrigated versus non-irrigated areas. The choice of reference period may affect the reconstructed irrigation effect on temperature, because of potentially varying temperature changes throughout the past century. Figure 5 shows that the reference period does not affect  $\Delta T_{irr}$  for most of the reference periods. A slightly stronger cooling can be observed for 1951-1980 with respect to the other reference periods.

## 6.3 Reconstructing the irrigation-induced temperature effect

### 6.3.1 CRU

The effect of irrigation on previous-century temperature changes can be calculated with the modified algorithm configuration obtained from a range of sensitivity studies detailed in the previous sections.

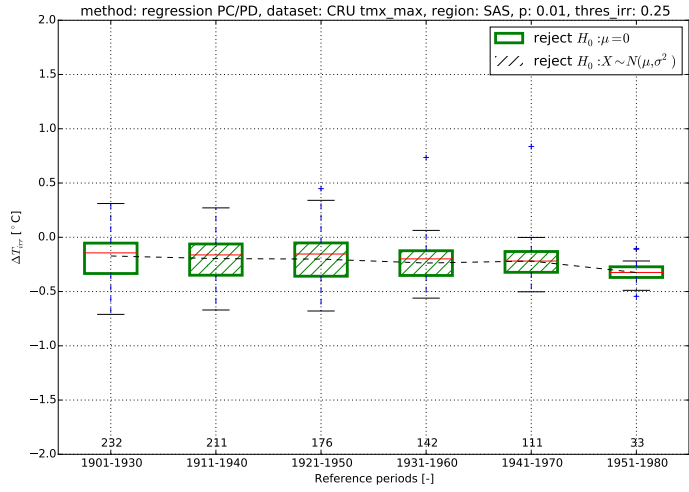


Figure 5: Reconstructed irrigation-induced temperature changes using the regression-based method on cells where  $\Delta f_{irr} \geq 0.25$  for different reference periods. Green boxes indicate samples where tests for the mean equal to 0 (Student's two-sided 1-sample T-test), and hatched boxes where  $H_0$  is that the sample can be drawn from a normal distribution (Shapiro-Wilk's non-parametric normality test) is rejected, both at a significance level of  $P \leq 0.01$ .

Global  $\Delta T_{irr}$  for CRU average diurnal maximum temperature in the hottest month of the year ( $TMX_{max}$ ) depicted in Figure 6 shows that the areas impacted by irrigation are mainly present in Asia, apart from small irrigated regions in Central and West North America (Figures 11 and 12 in Appendix A contain global spatial plots for other threshold values). The spatial distribution of  $\Delta T_{irr}$  in Asia (Figure 7) shows that the reconstructed temperature changes in South Asia are stronger than in East Asia. East Asian cooling is slightly underestimated compared to estimates by Shi *et al.* (2014). We note here that the threshold-based method shows more similarity between temperature changes in the two regions, although the cooling in South Asia remains stronger.

Contrastingly, the  $TMP_{max}$  signal shows distinct behavior in South Asia and East Asia. While South Asia experiences a reconstructed cooling, irrigation impacts temperature negligibly in East Asia (see Table 2). For South Asia, the magnitude of the temperature impact reconstructions is similar for both temperature variables, although a damped signal is expected because  $TMP_{max}$  reflects temperature extremes less than  $TMX_{max}$ . The underlying cause may be a data quality issue for CRU  $TMX_{max}$ ; this is further explained in the discussion. In East Asia, the damped signal for  $TMP_{max}$  with respect to  $TMX_{max}$  is shown as expected.

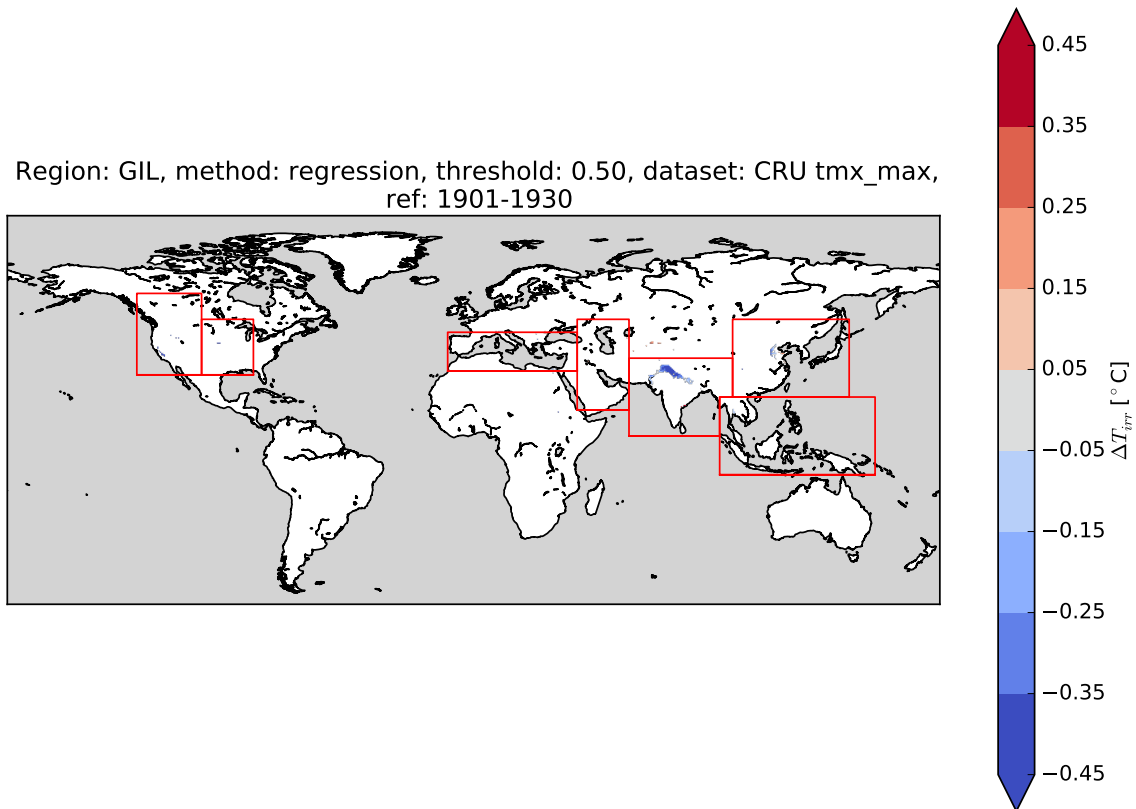


Figure 6: Reconstructed irrigation-induced change in temperature ( $CRU TMX_{max}$ ) for global irrigated land between 1901-1930 and 1981-2010 using a present-day irrigated cell fraction threshold of 0.5. Red boxes indicate SREX regions where irrigation-induced temperature changes can be expected based on [Thiery et al. \(2017\)](#).

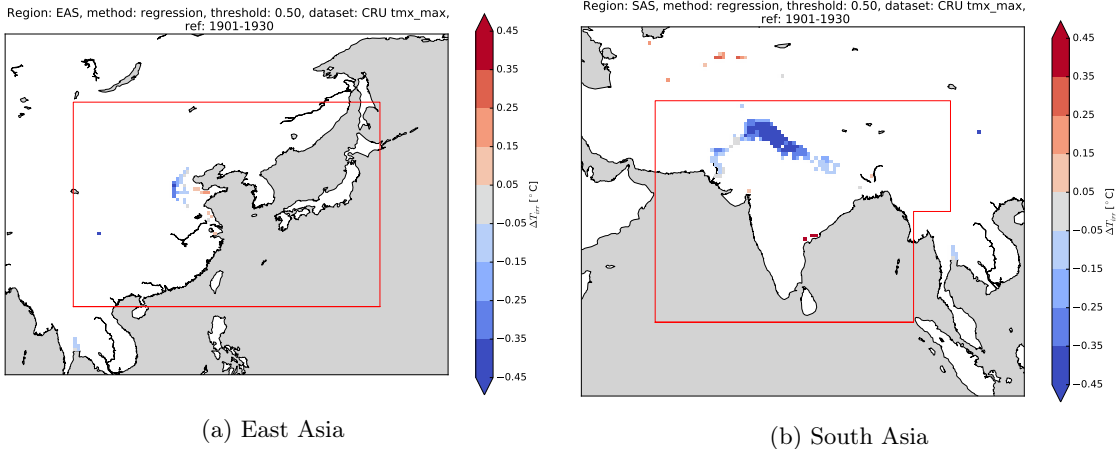


Figure 7: Similar to Figure 6, but for two SREX regions with widespread irrigation.

Table 2: Reconstructed  $\overline{\Delta T_{irr}}$  for two CRU variables in three regions, global irrigated land (GIL), East Asia (EAS) and South Asia (SAS), for two reference periods.

		GIL	EAS	SAS
$TMX_{max}$	1901-1930	-0.23	-0.10	-0.25
	1951-1980	-0.13	-0.04	-0.15
$TMP_{max}$	1901-1930	-0.17	0.05	-0.24
	1951-1980	-0.15	0.01	-0.22

### 6.3.2 HadEX2

Irrigation-induced changes in annual maximum daytime temperature ( $TXx$ ) suggest irrigation-induced cooling in India and, to some extent, North America (see Figure 8). The observed signal in India shows several strong positive  $\Delta T_{irr}$  values, which can be attributed to the low irrigation threshold of 0.05 or the coarse resolution of HadEX2 data. Spatial aggregation of irrigated fraction data to HadEX2 resolution ( $2.75^\circ \times 3.5^\circ$ ) results in a suboptimal representation of irrigation maxima in South and East Asia. Therefore, the irrigated fraction threshold of 0.5 has been changed to 0.05 (Figure 13 in Appendix A contains a global spatial plot for another threshold value).

HadEX2  $\Delta T_{irr}$  values are small in East China, and strongly positive in the Middle East. It is unclear whether this is a feature of the coarse HadEX2 resolution or an actual irrigation-induced effect. The small sample size limit statistically significant claims about irrigation-induced cooling at a regional scale for HadEX2.

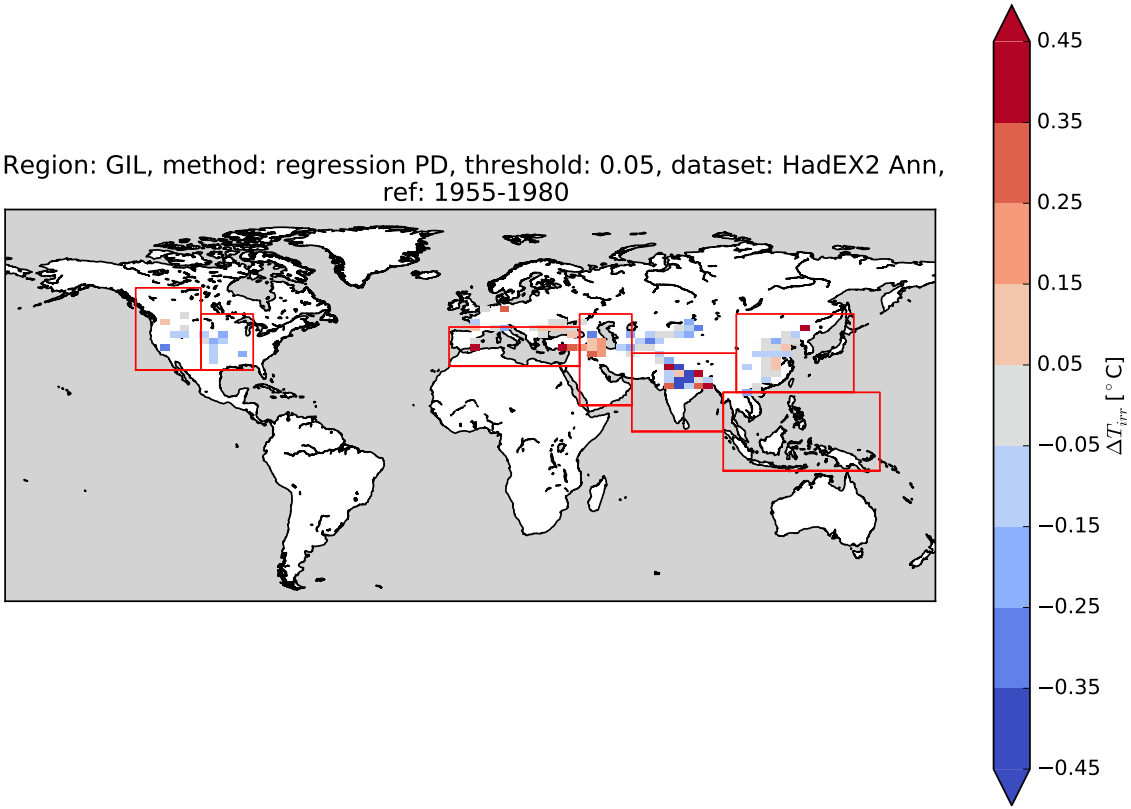


Figure 8:  $\Delta T_{irr}$  for HadEX2  $TXx$  between 1955-1980 and 1985-2010. Red boxes indicate SREX regions similar to Figure 6. HadEX2 temperature changes have been compared between two 26-year climatic time periods due to data inavailability up to 1955.

#### 6.4 Comparing CESM model output to CRU observations

The maximum monthly averaged daytime maximum surface temperature has also been extracted from CESM simulations and compared to CRU  $TMX_{max}$ . CESM consistently overestimates the cooling; particularly from irrigated fraction values of 0.5, the cooling is strongly overestimated by more than 1°C (see Figure 9a). Irrigated fraction values of 0.5 predominantly occur in South Asia, where station coverage is poor until 1955, which means the values are set to the climatology. Therefore, the variable  $TMX_{max}$  in South Asia does not reflect maximum daytime temperatures, but rather mean temperature. This can be seen in Figure 9, where the  $TMX_{max}$  signal for CRU differs only slightly from  $TMP_{max}$ . CESM  $TMP_{max}$  shows a damped signal compared to maximum temperatures, reducing the cooling overestimation to < 1°C.

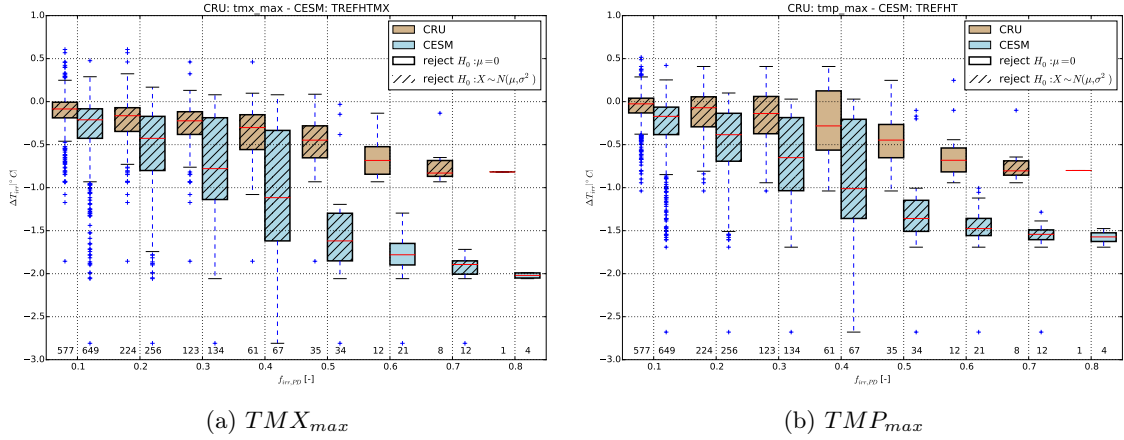


Figure 9: Comparison of the threshold dependence of  $\Delta T_{irr}$  between CRU (left, brown) and CESM (right, blue) for maximum daytime temperature and average temperature in the hottest month of the year. Black boxes and hatching respectively indicates a mean signal different from 0 (Student's two-sided one-sample T-test) and a non-normal distribution (Wilk-Shapiro test for normality) at a significance level of  $P \leq 0.01$ .

Despite the overestimation in reconstructed irrigation-induced cooling, Figure 10 shows that the total temperature change ( $\Delta T_{tot}$ ) for different present-day irrigation extents is more comparable. The agreement is particularly striking for large irrigated fraction values, where the irrigation effect on temperature suggests overestimation of the cooling by CESM.

The difference in  $\Delta T_{irr}$  either reflects the difference in irrigation in the reference period (CESM assumes no irrigation, whereas CRU takes the 1901-1930  $f_{irr}$  average of Siebert *et al.* (2015)) or that the model potentially represents regional irrigation impacts inadequately. For example, underestimated advection of air from irrigated areas to their surroundings would result in an overestimation of the temperature contrast between irrigated and non-irrigated land.

$t_{ref}$ : 1901-1930,  $t_{PD}$ : 1981-2010

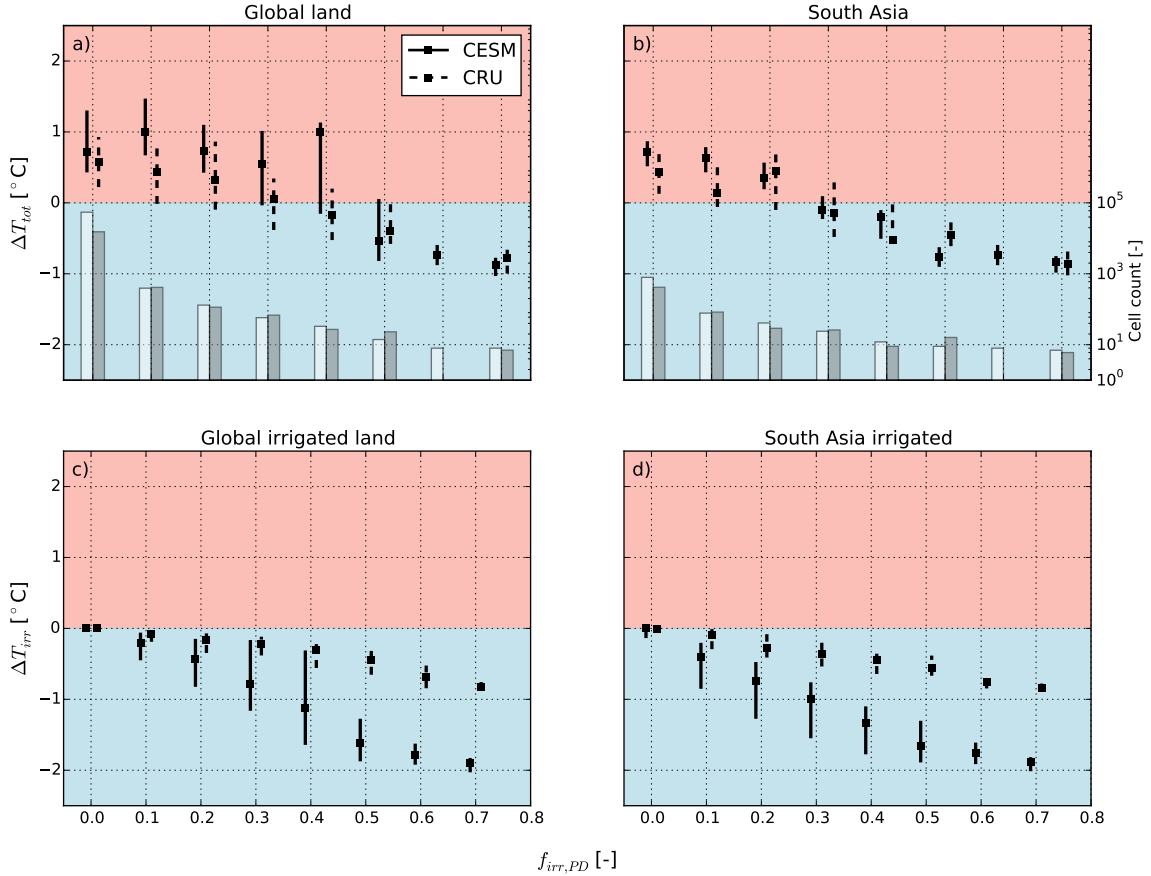


Figure 10: Boxplots of total  $TMX_{max}$  change ( $\Delta T_{tot}$ , upper panels) and irrigation-induced temperature change ( $\Delta T_{irr}$ , lower panels) for global land (left panels) and South Asia (right panels) between 1901-1930 and 1981-2010, binned by present-day (1981-2010) irrigated fraction. Cell count for  $\Delta T_{tot}$  is indicated in the upper panel for CESM (white) and CRU (grey).

## 7 Discussion

Several issues related to the temperature datasets and the window searching method limit this study. Firstly, temperature datasets are gridded and interpolated based on station observations. This implies that neighboring grid cells are not completely independent. Additionally, station coverage in irrigated areas ultimately determines whether an irrigation-induced temperature signal can be observed at all. One method to check this would be determine the station coverage in irrigated areas using the station locations of the temperature datasets.

Additionally, the resolution of temperature data sets is critical for detecting irrigation-induced temperature signals. Regridding the Historical Irrigation Dataset to the low resolution of HadEX2 aggregates much of the temperature signal, causing the irrigation values to be lower than for high-resolution datasets such as CRU. Additionally, the temperature signal itself is aggregated and there-

fore less likely to capture irrigation impacts.

Further issues arise when station coverage is not sufficient to have a representative coverage in certain regions. HadEX2 solves this by not reporting a measured temperature for those cells. CRU station coverage for mean temperature is sufficient to obtain global coverage: most cells are influenced by at least one station observation within approximately 850 km (Harris *et al.*, 2014). Fewer CRU stations report diurnal temperature range, which means that the composite variable maximum temperature ( $TMX_{max} = \max(TMP + \frac{1}{2} \times DTR)$ ) covers less grid cells, particularly for the period prior to 1955. Where station coverage is not sufficient, CRU reports the climatology (Thorne *et al.*, 2016). Therefore, reconstructed irrigation-induced temperature change signals in data-sparse regions reflect changes in  $TMP_{max}$  rather than  $TMX_{max}$ .

The applicability of the method to irrigation is limited by the violation of two of its assumptions. Firstly, the method assumes that the climate forcing of interest is spatially heterogeneous within the search window. Irrigation suitability is largely controlled by geographical features and therefore a clustered phenomenon. Additionally, the assumption that the climate forcing is purely local (i.e. only occurring in the cell of interest without any influence on surrounding cells) is likely violated, because of the non-local effects of irrigation. Cooler air might advect from irrigated cells to its surroundings, whereas the enhanced moisture content or cloud formation downwind of irrigated areas might influence temperature as well. These violations were relaxed by increasing the search window size, as explained in the Results section.

This study found underestimated irrigation-induced cooling compared to several other observation-based analysis using different methods (see e.g. Table 1 and Shi *et al.*, 2014; Lobell *et al.*, 2008). Additionally, the regression-based method yields underestimated irrigation-induced cooling compared to the threshold-based method. Lejeune *et al.* (2016) additionally found that the regression-based method underestimates results compared to factorial modelling experiments. It is plausible that this is caused by collinearity in the multi-linear regression (MLR) model: if  $\Delta f_{irr}$  is correlated with another predictor variable, the predictive power for individual regressors decreases. For example, elevation might be correlated with irrigation, because irrigation predominantly occurs in low-lying regions compared to their surroundings. Some preliminary tests with removing elevation from the equation did not reveal substantial and systematic changes in  $\Delta T_{irr}$ , but potential collinearity has not been ruled out.

The threshold-based approach could also introduce an underestimation in strongly cooled cells. All cells exceeding a threshold contribute to the signal in irrigated cells inside the search window, irrespective of their irrigated fraction. However, a stronger irrigation imprint on temperature is expected in cells with high irrigated fractions compared to cells that just exceed the irrigated fraction threshold.

## 8 Conclusions and Outlook

### Can a search window algorithm be applied to observational temperature estimates to quantify irrigation-induced cooling?

Two window searching algorithms were applied to irrigation and temperature datasets to quantify cooling from observations in the previous century. The algorithm can be applied to irrigation successfully, although one should keep in mind the limitations of the temperature datasets related to station density, interpolation and resolution. These factors might confound irrigation-induced temperature signals in gridded observational products.

We found that the method captures differential temperature responses in irrigated versus their non-irrigated surroundings, particularly for hot extremes, because 1) the reconstructed cooling is

strongest in irrigation hotspots in East and South Asia, and 2) the irrigation-induced cooling increases when using higher irrigated fraction thresholds for pixel selection

### **Can the algorithm configuration be modified to increase the observed direct climate effects of irrigation?**

Two modifications to the algorithm have increased the observed irrigation-induced cooling. Firstly, a differential criterion has been introduced for pixel selection and for the method itself. Pixels are currently selected based on their present-day irrigated fraction ( $f_{irr,PD}$ ), whereas the calculation of irrigation-induced cooling relies on changes in irrigated fraction ( $\Delta f_{irr}$ ) to reconstruct cooling in irrigated areas.

Secondly, a larger search window has been applied compared to previous studies. This relaxes the assumptions of the search window strategies related to heterogeneity of the local climate forcing inside the search window and the locality of the climate effect of the forcing.

### **By how much has irrigation affected surface temperatures in the previous century, and in which regions?**

Using a present-day irrigated fraction of threshold of 0.50, this study found that maximum daytime temperature in the hottest month of the year has changed by  $-0.25^{\circ}\text{C}$  in South Asia. The temperature change for global irrigated land is  $-0.23^{\circ}\text{C}$ , although this value is dominated by irrigation-induced temperature signals in South Asia.  $\Delta T_{irr}$  in East Asia is  $-0.04^{\circ}\text{C}$ , which is lower than a previously reported estimate by [Shi et al. \(2014\)](#).

### **How do irrigation estimates simulated by CESM and observed from CRU compare?**

CESM overestimates  $TMX_{max}$  compared to CRU by more than  $1^{\circ}\text{C}$  for irrigated fractions exceeding 0.5. As there is reason to doubt the representation of maximum daytime temperature in CRU, a comparison based on mean temperature in the hottest month of the year ( $TMP_{max}$ ) is more fair. This still yields an overestimation by CESM, although the magnitude is smaller ( $< 1^{\circ}\text{C}$ ).

## **Outlook**

This was a first attempt to globally quantify the effect of irrigation on surface temperature, where a statistically significant cooling was found that is most pronounced for strongly irrigated areas. Future work could focus on constraining irrigation-induced temperature signals better by applying the window searching methodology to regional temperature datasets with a higher station density, which have better-resolved temperature gradients between irrigated and non-irrigated areas. The regression-based window searching method can potentially still be improved, for example by correcting for the potential correlation between the spatial predictors irrigated fraction and elevation, and adding other spatial predictors such as urbanization.

A pairwise comparison between stations in irrigated- versus non-irrigated areas as performed by [Lobell et al. \(2008\)](#); [Shi et al. \(2014\)](#) better reflects local irrigation-induced temperature gradients. Establishing such a relation using station observation is a time-consuming task difficult to apply at a global scale, so this could be beneficial for regional studies into climate effects of irrigation.

Another fruitful direction for future research would be to study irrigation impacts on climate using satellite-based observations. One method would be to study local-scale spatial temperature contrasts induced by irrigation from land surface temperature measurements (as [Li et al. \(2015\)](#)

did for deforestation). Additionally, taking a similar approach as Teuling *et al.* (2017) could put observational constraints on enhanced cloud formation downwind of irrigated areas.

## References

- Bonfils, Céline, & Lobell, David. 2007. Empirical evidence for a recent slowdown in irrigation-induced cooling. *Proceedings of the National Academy of Sciences of the United States of America*, **104**(34), 13582–13587.
- Cook, Benjamin I., Puma, Michael J., & Krakauer, Nir Y. 2011. Irrigation induced surface cooling in the context of modern and increased greenhouse gas forcing. *Climate Dynamics*, **37**(7-8), 1587–1600.
- Donat, M. G., Alexander, L. V., Yang, H., Durre, I., Vose, R., Dunn, R. J H, Willett, K. M., Aguilar, E., Brunet, M., Caesar, J., Hewitson, B., Jack, C., Klein Tank, A. M G, Kruger, A. C., Marengo, J., Peterson, T. C., Renom, M., Oria Rojas, C., Rusticucci, M., Salinger, J., Elrayah, A. S., Sekele, S. S., Srivastava, A. K., Trewhin, B., Villarroel, C., Vincent, L. A., Zhai, P., Zhang, X., & Kitching, S. 2013. Updated analyses of temperature and precipitation extreme indices since the beginning of the twentieth century: The HadEX2 dataset. *Journal of Geophysical Research Atmospheres*, **118**(5), 2098–2118.
- Guimberteau, Matthieu, Laval, Katia, Perrier, Alain, & Polcher, Jan. 2012. Global effect of irrigation and its impact on the onset of the Indian summer monsoon. *Climate Dynamics*, **39**, 1329–1348.
- Harris, I., Jones, P. D., Osborn, T. J., & Lister, D. H. 2014. Updated high-resolution grids of monthly climatic observations - the CRU TS3.10 Dataset. *International Journal of Climatology*, **34**(3), 623–642.
- Kueppers, Lara M., Snyder, Mark A., & Sloan, Lisa C. 2007. Irrigation cooling effect: Regional climate forcing by land-use change. *Geophysical Research Letters*, **34**(3), 1–5.
- Kumar, Sanjiv, Dirmeyer, Paul A, Merwade, Venkatesh, Delsole, Timothy, Adams, Jennifer M, & Niyogi, Dev. 2013. Land use / cover change impacts in CMIP5 climate simulations : A new methodology and 21st century challenges. *Journal of Geophysical Research: Atmospheres*, **118**, 6337–6353.
- Lejeune, Quentin, Seneviratne, Sonia I, & Davin, Edouard L. 2016. *Historical land-cover change impacts on climate: comparative assessment of LUCID and CMIP5 multi-model experiments*.
- Lejeune, Quentin, Davin, Edouard L, Gudmundsson, Lukas, & Seneviratne, Sonia I. 2017. *Historical deforestation increased the risk of heat extremes in northern mid-latitudes*.
- Li, Yan, Zhao, Maosheng, Motesharrei, Safa, Mu, Qiaozhen, Kalnay, Eugenia, & Li, Shuangcheng. 2015. Local cooling and warming effects of forests based on satellite observations. *Nature communications*, **6**, 6603.
- Lobell, David B., Bonfils, Celine J., Kueppers, Lara M., & Snyder, Mark A. 2008. Irrigation cooling effect on temperature and heat index extremes. *Geophysical Research Letters*, **35**(9), 1–5.
- Mahmood, Rezaul, Keeling, Travis, Foster, Stuart A., & Hubbard, Kenneth G. 2013. Did irrigation impact 20th century air temperature in the High Plains aquifer region? *Applied Geography*, **38**(1), 11–21.
- Mueller, Nathaniel D., Butler, Ethan E., McKinnon, Karen A., Rhines, Andrew, Tingley, Martin, Holbrook, N. Michele, & Huybers, Peter. 2015. Cooling of US Midwest summer temperature extremes from cropland intensification. *Nature Climate Change*, **6**(3), 317–322.

- Puma, M. J., & Cook, B. I. 2010. Effects of irrigation on global climate during the 20th century. *Journal of Geophysical Research Atmospheres*, **115**(D16120), 15.
- Rodell, Matthew, Velicogna, Isabella, & Famiglietti, James S. 2009. Satellite-based estimates of groundwater depletion in India. *Nature*, **460**(7258), 999–1002.
- Sacks, William J., Cook, Benjamin I., Buenning, Nikolaus, Levis, Samuel, & Helkowski, Joseph H. 2009. Effects of global irrigation on the near-surface climate. *Climate Dynamics*, **33**, 159–175.
- Shi, Wenjiao, Tao, Fulu, & Liu, Jiyuan. 2014. Regional temperature change over the Huang-Huai-Hai Plain of China: The roles of irrigation versus urbanization. *International Journal of Climatology*, **34**(4), 1181–1195.
- Shukla, Sonali P., Puma, Michael J., & Cook, Benjamin I. 2014. The response of the South Asian Summer Monsoon circulation to intensified irrigation in global climate model simulations. *Climate Dynamics*, **42**(1-2), 21–36.
- Siebert, S., Döll, P., Hoogeveen, J., Faures, J.-M., Frenken, K., & Feick, S. 2005. Development and validation of the global map of irrigation areas. *Hydrology and Earth System Sciences*, **2**(4), 1299–1327.
- Siebert, Stefan, Kummu, Matti, Porkka, Miina, Döll, Petra, Ramankutty, Navin, & Scanlon, Bridget R. 2015. A global data set of the extent of irrigated land from 1900 to 2005. *Hydrology and Earth System Sciences*, **19**(3), 1521–1545.
- Teuling, Adriaan J., Taylor, Christopher M., Meirink, Jan Fokke, Melsen, Lieke A., Miralles, Diego G., van Heerwaarden, Chiel C., Vautard, Robert, Stegehuis, Annemiek I., Nabuurs, Gert-Jan, & de Arellano, Jordi Vilà-Guerau. 2017. Observational evidence for cloud cover enhancement over western European forests. *Nature Communications*, **8**, 14065.
- Thiery, Wim, Davin, Edouard L., Lawrence, David M., Hirsch, Annette L., Hauser, Mathias, & Seneviratne, Sonia I. 2017. Present-day irrigation mitigates heat extremes. *Journal of Geophysical Research: Atmospheres*, available online.
- Thorne, P. W., Donat, M. G., Dunn, R. J H, Williams, C. N., Alexander, L. V., Caesar, J., Durre, I., Harris, I., Hausfather, Z., Jones, P. D., Menne, M. J., Rohde, R., Vose, R. S., Davy, R., Klein-Tank, A. M G, Lawrimore, J. H., Peterson, T. C., & Rennie, J. J. 2016. Reassessing changes in diurnal temperature range: Intercomparison and evaluation of existing global data set estimates. *Journal of Geophysical Research: Atmospheres*, **121**(10), 5138–5158.

# Appendices

## A Auxiliary figures

Many other figures have been created besides those shown in the report. A selection of figures will be shown in this appendix. These figures are also stored at `/net/firebolt/data/viserra/Figures`.

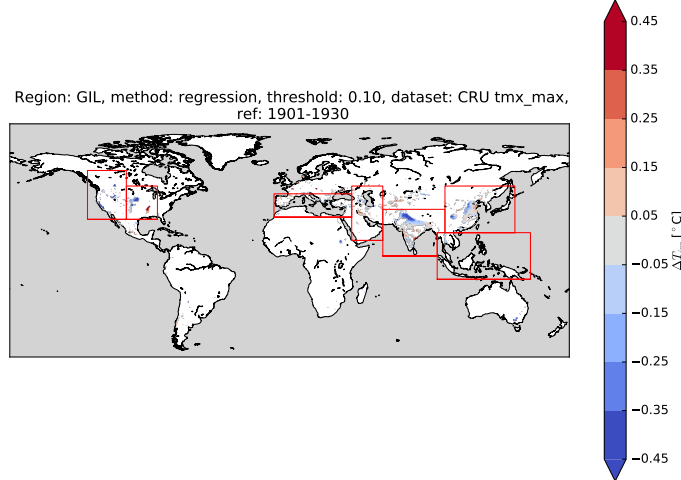


Figure 11: CRU irrigation-induced temperature change  $\Delta T_{irr}$  for global irrigated land between 1901-1930 and 1981-2010 calculated using the regression-based method using a pixel selection threshold of 0.1

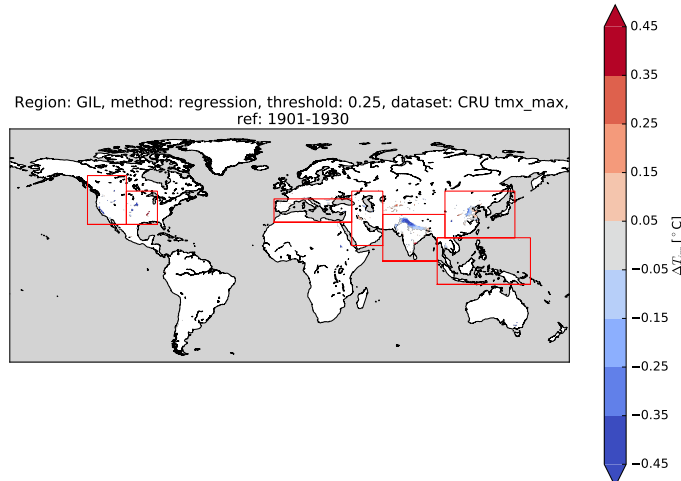


Figure 12: CRU irrigation-induced temperature change  $\Delta T_{irr}$  for global irrigated land between 1901-1930 and 1981-2010 calculated using the regression-based method using a pixel selection threshold of 0.25

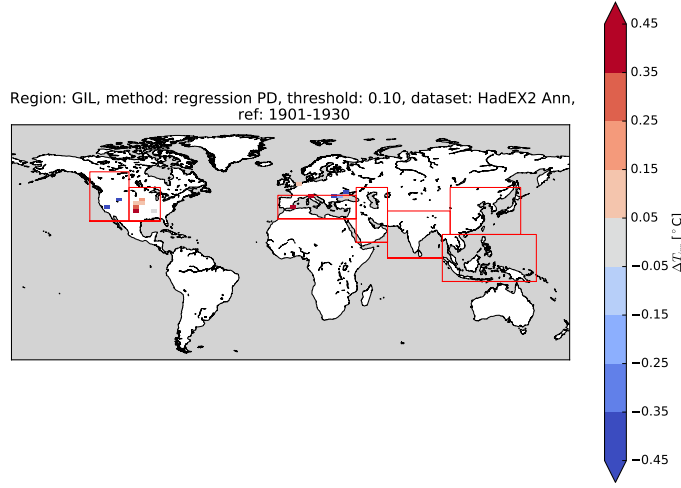


Figure 13: HadEX2 irrigation-induced temperature change  $\Delta T_{irr}$  for global irrigated land between 1901-1930 and 1981-2010 calculated using the regression-based method using a pixel selection threshold of 0.1

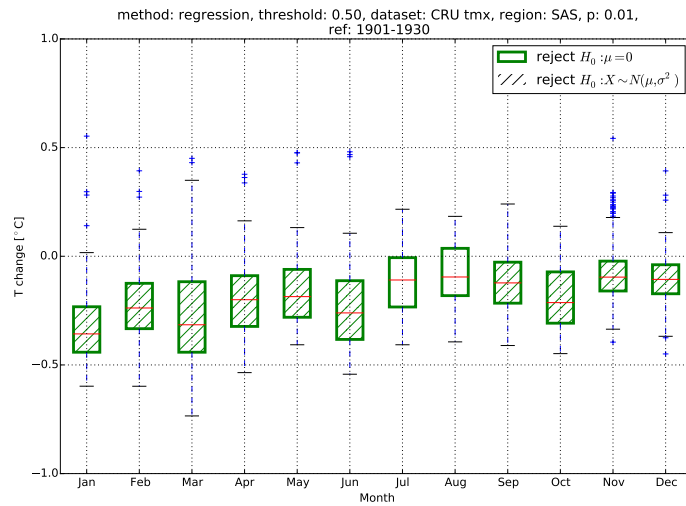


Figure 14: Monthly boxplots for CRU *tmx* calculated using the regression-based method with a pixel selection threshold of 0.5, between 1901-1930 and 1981-2010.

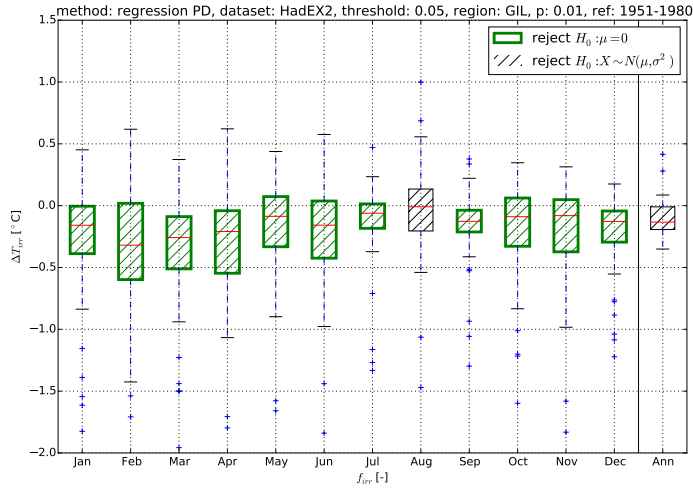


Figure 15: Monthly boxplots for HadEX2 maximum monthly temperature calculated using the regression-based method with a threshold of 0.01 between 1951-1980 and 1981-2010.  $\Delta T_{irr}$  for  $TXx$  is given on the right ('Ann').

## B Python scripts

The analyses have been performed using Python. The threshold- and regression-based algorithms are coded in four files, and the rest of the files contain scripts that execute the method based on a range of user-specified input and generate plots. All scripts are saved at `/net/firebolt/data/vissera/scripts/`. The data needed to run the script is either accessed directly from `/net/exo/landclim/data/dataset/` or, for regridded HID data using CDO commands, stored at `/net/firebolt/data/vissera/Data/`.

### B.1 The window searching algorithms

The algorithm files all contain one function, which can be called from other algorithm or plotting scripts. The algorithm is written in the following four files:

- `extract_T_irr.py` extracts the 30-year mean gridded temperature for two periods specified by the user and stores it in a three- ( $2 \times n_{lat} \times n_{lon}$ ) or four-dimensional ( $2 \times n_{seasons/months} \times n_{lat} \times n_{lon}$ ) array dependent on the chosen temperature index. CRU generates four-dimensional outputtemperature can be analyzed at monthly or seasonal resolution.
- `calc_irr_diff.py` generates a three-dimensional array of 30-year averaged irrigation maps for the reference and present-day periods.
- `calc_irr_impact_threshold.py` contains a function calculates irrigation-induced temperature change ( $\Delta T_{irr}$ ) using the threshold-based method based on a range of user-specified parameter choices.
- `calc_irr_impact_regression.py` contains a function calculates irrigation-induced temperature change ( $\Delta T_{irr}$ ) using the regression-based method based on a range of user-specified parameter choices.

## B.2 Relevant plotting scripts

The plotting scripts all contain a section on top where the user can choose variables for the analysis, e.g. the temperature dataset, the temperature product or the analysis periods. The following files are most relevant for generating plots (scripts work for all temperature datasets unless indicated otherwise):

- `dT_irr_SREX.py` executes one of the algorithms using parameter choices selected by the user and prints or generates spatial plots of the results. Alternatively, `dT_irr_SREX.py` can generate monthly boxplots for CRU. Note: the boxplot commands generates different results depending on the temperature dataset and variable. For CRU monthly, the annual cycle is plotted. For CRU seasonal and  $TMX_{max}$  (and similar variables), the script shows boxplots containing  $\Delta T_{irr}$  for the different SREX regions.
- `dT_asfuncof_thres.py` calculates  $\Delta T_{irr}$  for a range of threshold values and plots the results as boxplots.
- `SREX_scatter_binned.py` generates binned boxplots for the total temperature change ( $\Delta T_{tot}$ ) for global irrigated land (GIL) and seven SREX regions.
- `CRU_CESM_binnedboxplotRegional.py` calculates  $\Delta T_{tot}$  and  $\Delta T_{irr}$  for global land and a user-selected region (currently only works for South Asia).
- `CESM_CRU_comp.py` calculates  $\Delta T_{irr}$  for a range of threshold values for CESM and CRU regridded to CESM resolution, and plots the results as boxplots.
- `monthlyboxplots.py` generates monthly boxplots for HadEX2.

The parameters that users can modify are:

- `SREX_region` is the SREX region for which the results will be calculated
- `plot_season` and `plot_month` are the season/month of interest if CRU is analyzed at a seasonal/monthly resolution
- `yr_start1`, `yr_end1`, `yr_start2` and `yr_end2` determine the reference and present-day period
- `method`: 'regression' or 'threshold'
- `thres_irr` is the irrigated fraction threshold used for pixel selection
- `u` is the scaling factor by which `thres_irr` is multiplied to obtain the pixel separation criterion for the threshold-based method
- `datasource` is the temperature datasource used in the analysis. Possible choices are CRU, HadEX2, CESM and CRU\_CESM (CRU regridded to CESM resolution)
- `temp_product` is the temperature product. Possible choices are given in the script `dT_irr_SREX.py`
- `response` can be 'PC/PD' if pixel selection should occur by changes in irrigated fraction, or 'PD' if pixels should be selected based on  $f_{irr,PD}$
- `t_res` is the temporal resolution for the analysis ('seasonal' or 'monthly')

- **def\_regr** is a boolean switch that determines whether deforestation should be included in the multi-linear regression for the threshold-based method.
- **scaling** determines whether the threshold-based results should be collapsed to their mean value and scaled by  $\Delta f_{irr}$  to obtain  $\Delta T_{irr}$ .
- **p\_value** is the p-value to be used for significance tests.
- **figsave** is a boolean switch that determines whether the figure is saved.
- **figformat** determines the format of the plot (e.g. 'png' or 'pdf').